Journal of Colloid and Interface Science 667 (2024) 338–349

Contents lists available at ScienceDirect

Journal of Colloid And Interface Science

journal homepage: www.elsevier.com/locate/jcis

Regular Article

Extracellular vesicles selective capture by peptide-functionalized hollow fiber membranes

Simona Salerno [a,1], Antonella Piscioneri [a,1], Sabrina Morelli [a], Alessandro Gori [b], Elena Provasi [c], Paola Gagni [b], Lucio Barile [d,e], Marina Cretich [b], Marcella Chiari [b], Loredana De Bartolo [a,*]

[a] Institute on Membrane Technology, National Research Council of Italy, ITM-CNR, via P. Bucci, cubo 17/C, I-87036 Rende (CS), Italy
[b] Institute of Chemical Sciences and Technologies "G. Natta", National Research Council of Italy, SCITEC-CNR, Via Mario Bianco 9, 20131, Milan, Italy
[c] Lugano Cell Factory, Istituto Cardiocentro Ticino, Ente Ospedaliero Cantonale, via Tesserete 48, 6900 Lugano, Switzerland
[d] Cardiovascular Theranostics, Istituto Cardiocentro Ticino, Laboratories for Translational Research, Ente Ospedaliero Cantonale, Via Chiesa 5, 6500 Bellinzona, Switzerland
[e] Euler Institute, Faculty of Biomedical Sciences, Università della Svizzera Italiana (USI), Via Buffi 13, 6900 Lugano, Switzerland

HIGHLIGHTS

- HF membranes are modified by a nanometric coating with a copoly azide polymer to limit non-specific interactions and to enable the conjugation with peptide ligand by click chemistry reaction.
- Peptide-functionalized hollow fiber membranes are effective for the separation and enrichment of highly pure EVs.
- TFF integrated BPt-functionalised membrane module is able to selectively capture EVs with diameter < 200 nm.
- The BPt-functionalised membrane module integrated in a TFF process allowed to remove contaminants molecules.
- The functionalization strategy allows to revert the peptide-EVs interaction triggering the release of captured vesicles.

GRAPHICAL ABSTRACT

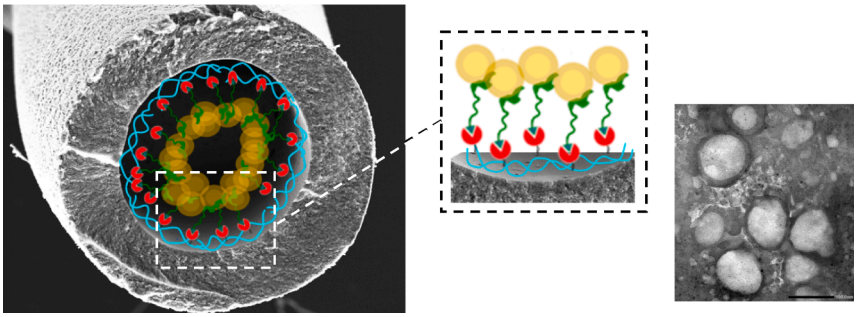

ARTICLE INFO

Keywords:
Hollow fiber membranes
Peptide functionalization
Tangential flow filtration
Extracellular vesicles
Isolation
Cell culture

ABSTRACT

Recently, membrane devices and processes have been applied for the separation and concentration of subcellular components such as extracellular vesicles (EVs), which play a diagnostic and therapeutic role in many pathological conditions. However, the separation and isolation of specific EV populations from other components found in biological fluids is still challenging. Here, we developed a peptide-functionalized hollow fiber (HF) membrane module to achieve the separation and enrichment of highly pure EVs derived from the culture media of human cardiac progenitor cells. The strategy is based on the functionalization of PSf HF membrane module with BPt, a peptide sequence able to bind nanovesicles characterized by highly curved membranes. HF membranes were modified by a nanometric coating with a copoly azide polymer to limit non-specific interactions and to enable the conjugation with peptide ligand by click chemistry reaction. The BPt-functionalized module was

* Corresponding author at: National Research Council of Italy, Institute on Membrane Technology, CNR-ITM, Via P. Bucci cubo 17/C, I-87030 Rende (CS), Italy.
E-mail addresses: l.debartolo@itm.cnr.it, loredana.debartolo@cnr.it (L. De Bartolo).
[1] These authors contributed equally.

https://doi.org/10.1016/j.jcis.2024.04.074
Received 4 January 2024; Received in revised form 8 April 2024; Accepted 10 April 2024
Available online 12 April 2024
0021-9797/© 2024 The Author(s). Published by Elsevier Inc. This is an open access article under the CC BY license (http://creativecommons.org/licenses/by/4.0/).

integrated into a TFF process to facilitate the design, rationalization, and optimization of EV isolation. This integration combined size-based transport of species with specific membrane sensing ligands. The TFF integrated BPt-functionalized membrane module demonstrated the ability to selectively capture EVs with diameter < 200 nm into the lumen of fibers while effectively removing contaminants such as albumin. The captured and released EVs contain the common markers including CD63, CD81, CD9 and syntenin-1. Moreover, they maintained a round shape morphology and structural integrity highlighting that this approach enables EVs concentration and purification with low shear stress. Additionally, it achieved the removal of contaminants such as albumin with high reliability and reproducibility, reaching a removal of 93%.

1. Introduction

There is a growing interest in membranes and membrane processes within biomedical applications, especially in various life-saving treatments. The increasing need for high purity products, the global prevalence of diseases, and the expanding life science and healthcare industry are key factors propelling this growth. Membranes find utility in diverse applications, including drug delivery, artificial organs, tissue regeneration, diagnostic devices, and bioseparations [1–5]. More recently, membrane processes have been employed for the separation and concentration of subcellular components such as extracellular vesicles (EVs), which play a pivotal diagnostic and therapeutic role [6] in numerous pathological conditions.

EVs have emerged as important mediators, potentially constituting a new signalling paradigm in intercellular communication. Secreted by cells, they carry diverse cargoes comprising proteins, RNA species, DNAs, and lipids. These cargoes which can be delivered to recipient cells, influencing the phenotype of these cells at both paracrine and systemic levels. The capacity to transfer or deliver messages from one cell to another renders EVs promising candidates for therapeutic purposes. EVs play a role in the regulation of normal and pathological processes, encompassing cancer, neurodegeneration, cardiovascular and inflammatory diseases [7–10]. They can be considered significant biomarkers for disease diagnosis and therapeutic monitoring and can be used as therapeutic delivery vehicles to reverse pathological phenomena.

The most used methods for EV isolation are based on four classes of isolation techniques including ultracentrifugation, size-based isolation (e.g., size exclusion chromatography and ultrafiltration), immunoaffinity and precipitation [11]. Since each method has its unique advantages and disadvantages (e.g., low yields, not scalable, low purity) considerable efforts have been devoted to improving EVs isolation and purification. Currently, one of the best options is the combination of different methods in EV isolation due to their different source and heterogeneity [11,12]. Advances in membrane science and surface modification strategies have led to the integration of size-exclusion mechanisms with specific ligands probes. Recently, we developed a functionalized polysulfone (PSf) tangential flow filtration (TFF) flat membrane unit capable of binding lipid nanovesicles while avoiding the binding of contaminants and other non-target molecules [13]. The membrane underwent modification through the application of a coating comprising a copolymer with azide functionality. This coating serves to limit non-specific interactions and enables the functionalization with peptide bioprobes through a click chemistry reaction. The peptide BPt, derived from bradykinin, exhibits efficient binding to both synthetic and biogenic lipid nanovesicles characterized by highly curved membranes (<150 nm), including small EVs [14,15]. The BPt-functionalized membrane exhibited a remarkable capturing efficiency towards synthetic liposomes enhancing filtration performance and antifouling capacity.

The success of this strategy prompted its application to the separation, enrichment, and release of cell-derived EVs.

In this context, we proposed a readily scalable approach for achieving the separation and enrichment of highly pure EVs, utilizing a BPt-functionalized hollow fiber (HF) membrane module. The HF PSf membrane modules were modified by a nanometric coating of copoly azide polymer Copoly (DMA-NAS-N_3-MAPS) derived from the post-polymerization modification of the parental copolymer copoly-(DMA-NAS-MAPS). This copolymer is composed of N,*N*-dimethylacrylamide (DMA), 3-(trimethoxysilyl)propyl methacrylate (MAPS), and *N*-acryloyloxysuccinimide (NAS) [16,17]. The copoly-azide polymer coating allows functionalizing the surface membrane with orthogonal functional groups that enable the controlled conjugation of peptide ligands for EVs capture. The BPt peptide (sequence: RPPGFSPFR-(O_2Oc)-RPPGFSPFR-K-G-(O_2Oc)$_2$-Prg), belongs to the family of membrane curvature sensing peptides (MSP). More in general, this class of peptides is conceptually derived from associated curvature sensor domains in proteins [18]. A common feature among different MSP sequences is their amphipathic character, driving a selective binding to relatively small (bio)nanovesicles through the combination of electrostatic and hydrophobic interactions. While still debated, it is widely assumed that the initial recognition is driven by electrostatic complementarity between positive residues in the peptide and negatively charged head groups of membrane lipids, which then facilitates the insertion and folding of the peptide within loosely packed membrane bilayers, characteristic of highly curved structures. Here BPt sequence was selected based on previous promising applications in both analysis and isolation of EVs [15]. The idea is to combine size and affinity isolation and to achieve at the same time the selective isolation and concentration of EVs with a size < 200 nm, which are most intensively investigated for their role in various pathophysiological processes. To this purpose we functionalized membranes in HF configuration in order to provide the highest surface area per unit volume, compactness and modular design, all characteristics that influence separation efficiency and application. In such configuration the fluid flow is applied tangentially to the membrane lumen to prevent the accumulation of targeted components and filter clogging issues, which reduce the number of open pores and change the hydrodynamic conditions. Membrane properties including structural, physical–chemical, and permeability properties were characterized to optimize the separation process. The BPt functionalization of membranes enables the implementation of isolation and enrichment of a specific range of EVs integrating the size-based transport of species with specific membrane-sensing ligands. Additionally, the functionalization strategy allows the peptide-EVs interaction to be reverted, triggering the release and delivery of the vesicles after treatment with divalent metal cations.

The isolation efficiency of the BPt functionalized HF membranes under TFF process was demonstrated by using a heterogeneous EV population derived from the culture media of human cardiac progenitor cells (hCPCs) cultured up to 14 days compliant with current good manufacturing practices (cGMP) [19,20].

2. Materials and methods

2.1. Polymer synthesis and characterization

Copoly (DMA-NAS-N_3-MAPS) was obtained by post-polymerization modification of the parental copolymer Copoly (DMA-NAS-MAPS) that was previously synthesized by free radical polymerization, as reported in the literature [21]. Briefly, after degassing anhydrous THF with Argon, DMA, NAS, and MAPS were added to the reaction flask so that

their molar fraction was respectively 89:10:1 and the concentration of the total monomer was maintained at 20% w/v. Then, α, α′-azoisobutyronitrile (AIBN) was added as a radical initiator, and the reaction mixture was heated to 65 °C for two hours. The crude material was cooled to room temperature and diluted 1:1 with dry THF; the solution was then precipitated in petroleum ether (10 times the volume of the reaction mixture) to eliminate unreacted monomers. The polymer was collected by filtration as a white powder and dried under vacuum at room temperature.

The introduction of azido functionality was carried out as previously described [16]. A partial substitution of NAS moieties was obtained by adding 11-Azido-3,6,9-trioxaundecan-1-amine (molar ratio NAS/azido linker 0.5). Copoly (DMA-NAS-MAPS) was dissolved into anhydrous THF to a final concentration of 10% w/v, and the corresponding amount of 11-Azido-3,6,9-trioxaundecan-1-amine was added to the feed. After five h, the solution was poured into petroleum ether and recovered as described above.

Copoly (DMA-NAS-N_3-MAPS) and Copoly (DMA-NAS-MAPS) polymers have been characterized by acquiring ^{13}C NMR spectra at 500 MHz Bruker Avance II and 600 MHz Bruker Avance DRX spectrometers equipped with reverse 5 mm TXI probe with z gradient. About 30 mg of polymer were dissolved in DMSO–d_6 solvent. All spectra were recorded at 300 K and calibrated on solvent signal resonating at 2.5 ppm (^1H) and 40.5 ppm (^{13}C).

2.2. Peptide synthesis and characterization

Peptide was assembled by stepwise microwave-assisted Fmoc-SPPS on a Biotage ALSTRA Initiator+ peptide synthesizer, operating in a 0.05 mmol scale. Activation of entering Fmoc-protected amino acids (0.3 M solution in DMF) was performed using 0.5 M Oxyma in DMF/0.5 M DIC in DMF (1:1:1 M ratio), with a 5-equivalent excess over the initial resin loading. Coupling steps were performed for 45 min at 50 °C. Capping steps were performed by treatment with a 0.3 M Ac_2O/0.3 M DIEA solution in DMF (1 x 5 min). Fmoc- deprotection steps were performed by treatment with a 20% piperidine solution in DMF at room temperature (1 x 10 min). Following each coupling, capping or deprotection step, peptidyl-resin was washed with DMF (3 x 3.5 mL). Upon complete chain assembly, resin was washed with DCM (5 x 3.5 mL) and gently dried under nitrogen flow. Resin-bound peptide was treated with an ice-cold TFA, TIS, water, thioanisole mixture (90:5:2.5:2.5 v/v/v/v, 3 mL). After gently shaking the resin for 2 h at room temperature, the resin was filtered and washed with neat TFA (2 x 4 mL). Cleavage mixture was concentrated under nitrogen stream and then added dropwise to ice-cold diethyl ether (40 mL) to precipitate the crude peptide. The crude peptide was collected by centrifugation and washed with further cold diethyl ether to remove scavengers. Peptide was then dissolved in 0.1% TFA aqueous buffer (with minimal addition of ACN to aid dissolution, if necessary). Residual diethyl ether was removed by a gentle nitrogen stream. Analytical and semi-preparative reversed-phase high-performance liquid chromatography (RP-HPLC) were then carried out on a Shimadzu Prominence HPLC system equipped with a multichannel detector. A Phenomenex Jupiter 5μ C18 90 Å column (150 x 4.6 mm) was used for analytical runs and a Phenomenex Jupiter 10 μ C18 90 Å (250 x 21.2 mm) for peptide purification. Data were recorded and processed with LabSolutions software. 5–100% linear gradient eluent B at a flow rate of 0.5 mL/min was used for analytic purposes (20 min run). Eluent A = H_2O/3% CH_3CN/0.07% TFA, eluent B = 70% CH_3CN/30% H_2O/0.07% TFA. Peptide purification was achieved by preparative RP-HPLC at a flow rate of 14 mL/min using a 100% A→ 30% B gradient over 40 min. Pure RP-HPLC fractions (>95%) were combined and lyophilized. Mass spectra were collected separately on a Shimadzu LC-MS2020 instrument. Reagents for peptide synthesis were from Iris Biotech (Marktredwitz, Germany).

2.3. Hollow fiber membrane module

The hollow fiber cartridges for laboratory-scale cross flow filtration (Cytiva, Europe GmbH), comprises six hollow fiber membranes with nominal molecular weight cut-off of 500 kDa and a total area of 26 cm^2.

The device (hollow fiber ultrafiltration cartridge) underwent to a rinsing procedure in order to ensure the removal of glycerol preservative, which was used to prevent drying of the membrane. The first step of the rinsing procedure consisted in pumping through the cartridge a solution of 25% ethanol at the pressure of 0.3 bar for 10 min, afterwards the ethanol filled cartridge was left to soak for 1 h. The ethanol was then drained and discarded. To finalize the procedure the module was rinsed for 90 min with clean pure water at a working pressure of 0.3 bar.

The permeability properties of HF cartridge were characterized by pure water flux measurements at different *trans*-membrane pressures (ΔP^{TM}). For each HF cartridge was assessed the hydraulic permeance L_P by applying the following equation:

$$L_P = \left(\frac{J_{Solvent}}{\Delta P^{TM}}\right)_{\Delta c=0}$$

This equation provides a linear correlation between water flux and the convective driving force. Therefore, the steady-state hydraulic permeance of the HF membranes was calculated according to the slope of the flux J vs the transmembrane pressure (ΔP^{TM}).

Hydraulic performance measurements confirmed that the glycerol was moved away from membrane pores, since the assessed pure water permeability was in the same range permeability specification established by Cytiva. Thus, after the cleaning procedure the HF cartridge was modified for the EVs capture. After the cleaning procedure the permeability performance was always assessed to ensure a proper membrane functionalization.

The physico-chemical properties of the native HF and BPt functionalized HF membranes were characterized to evaluate their hydrophobicity/hydrophilicity by performing water contact angle (WCA) measurements in static condition by using Contact Angle Meter, CAM 200 (KSV Instrument LTD, Helsinki, Finland). The contact angle measurements were performed on the outer surface of the hollow fiber membranes due to the small size of lumen diameter (500 μm). As control, contact angle was also measured on the same PSf membrane in flat configuration that displayed the same values. The comparison of the values before and after surface modification with copoly azide polymer and peptide conjugation highlights the effective change of the physico-chemical properties.

The surface tension γ of the membranes and its components were calculated as function of the average values of contact angle in three different reference liquids, by application of the Good–van Oss approach [22], as previously reported [23]. In brief, the contact angle in diiodomethane, as an apolar test liquid, was used to calculate the apolar Lifshitz–van der Waals component (γ^{LW}). Then, the other components of the membrane surface tension, namely acid (γ^+), base (γ^-) and acid–base (γ^{AB}), were determined by using two polar liquids: glycerol and water. The CA in the test liquids was randomly measured on different areas of the sample surface and the results were expressed as mean ± SEM from 10 measurements.

2.4. HF membrane functionalization

The lumen surface of the HF membranes was functionalized with Copoly (DMA-NAS-N_3-MAPS)-BPt peptide conjugation, as previously reported [13]. To achieve a homogeneous coating layer and the proper peptide binding it was used an amount of copolymer and peptide of 4.3 mg/cm^2 and 150 μg/cm^2, respectively. Briefly, membranes were pretreated with NaOH 1 M for 30 min, and, after a washing, with HCl 1 M for 30 min. Then the HF membranes were filled with 0.4 mL of the copolymer c-(DMA-NAS-N_3-MAPS) 27.8% (w/v) in 10% $(NH_4)_2SO_4$, and maintained for 1 h at RT. After that, the excess polymer solution was removed, and the coated polymer cured at 80 °C for 20 min, rinsed with

distilled water, and finally dried at 40 °C for 1 h. Thereafter, the peptide binding of the polymer-coated membranes was carried out by filling the HF cartridge with 0.4 mL of BPt (RPPGFSPFR-$(O_2Oc)_2$ −RPPGFSPFR-KG $(O_2Oc)_2$-Prg 2.78 mM in 18.5x concentrated click buffer solution (1.85 mM $CuSO_4$, 7.41 mM THTPA, 115.83 mM ascorbic acid), and maintaining overnight at RT. Finally, the excess of peptide solution was eliminated, and the membranes rinsed twice with distilled water, and dried at 40 °C for 30 min.

2.5. Production and concentration of EVs from human cardiac progenitor cells

EVs have been produced following state-of-the-art procedures, compliant with GMP-grade large-scale protocols as for Andriolo et al [24]. Briefly aliquots of human cardiac progenitor cells (hCPCs) from established master cell bank (MCB) [19], were thawed and expanded for two passages in StemMACS-MSC expansion Media kit XF (Miltenyi Biotec GmbH, Germany). Once cells reached 80% of confluence cell-expanding medium has been exchanged with EV producing medium, Dulbecco's Modified Eagle Medium (DMEM) 4.5 g/L glucose without phenol red (Gibco/Thermo Fisher Scientific). Upon 14 days of culture, the conditioned medium (CM) was harvested and clarified by ULTRA Pure HC 0.6/0.2 μm filter (GE Healthcare) to deplete floating cells and large cell debris. EVs concentration was performed by size exclusion tangential flow filtration (TFF), using the ÄKTA™ flux 6 system (GE Healthcare) equipped with a 300 kDa cut-off hollow fiber cartridge (GE Healthcare). The size exclusion TFF allowed to concentrate EVs and deplete contaminants that are smaller of 300 kDa (cartridge cut-off).

This method was applied during process scale up and for the large-scale manufacturing of GMP-Exo-CPC. After production, EVs have been characterized by NTA, TSG101 ELISA and superficial tetraspanin expression by FACS.

2.6. Integration of BPt –functionalized membrane with TFF for EVs capture and release

The functionalized HF membrane module was used for the EVs capture by TFF, connecting it to the experimental set-up that consists of tubes, a peristaltic pump and two pressure gauges at the inlet and outlet streams. A feed solution (27 mL) containing EVs $3.3*10^9$ part/mL in sterile and filtered PBS, was fed to the lumen of the HFs at a flow rate of 2 mL/min, in order to maintain a transmembrane pressure ΔP^{TM} of 25 mbar, continuously monitored by the pressure gauges. The average residence time of the EV solution inside the module was 1.2 min. The TFF, or cross-flow filtration, allows the separation of species that pass through the membrane in the permeate, from the rest, the retentate, that is cut off and recycled back to the feed. After 60 min, 17 mL of permeate and 10 mL of retentate were collected, respectively. In the meantime, the EVs capture was ensured by the specific binding with the BPt peptide over the functionalized membrane surface [17]. Thereafter, for the release of the captured EVs, the permeate was closed, and the cartridge filled with 6.8 mL of $MgCl_2$ 500 mM, that was continuously recycled for 60 min at a flow rate of 2 mL/min. This $MgCl_2$ concentration was selected upon preliminary screening of a range of concentrations (10 mM – 1 M), as resulted in the lowest $MgCl_2$ amount yielding consistent results. While characterizing in detail the mechanisms by which $MgCl_2$ induces the release of EVs remains arduous in such a complex system, we speculate that the divalent Mg^{2+} cation can either coordinate polar groups on both the peptide and the membrane, shielding mutual supramolecular interactions and loosening their binding affinity.

2.7. EVs captured/released quantification

The EVs captured and successively released in the process were quantified in the feed and in the $MgCl_2$ eluted solutions, and in the collected retentate and permeate, by ELISA assays of EV-specific tetraspanins, TSPAN30 or CD63, TSPAN29 or CD9, TSPAN28 or CD81, and syntenin-1 (Cloud-Clone Corp.), according to manufacturer's instructions.

The ability of the TFF process to remove contaminant proteins was assessed by quantifying albumin in the feed and in the $MgCl_2$ eluted solutions, and in the collected retentate and permeate, by immunoenzymatic ELISA test [25]. For the assay, 100 μL of samples were incubated at 4 °C overnight with 100 μL of anti-human albumin monoclonal antibody conjugated with horseradish peroxidase (Bethyl Laboratories, Inc., USA) in 96 well plates previously coated with 50 μg/mL chromatographically purified human albumin (Sigma, Milan, Italy). After 4 washes, the enzymatic reaction was run for 7 min by adding tetramethylbenzidine (Sigma, Milan, Italy) and H_2O_2 as detection substrates, and then stopping with 8 N H_2SO_4. Absorbance was measured at 450 nm using a Multiskan Ex (Thermo Lab Systems).

2.8. SiMoA assay

The SiMoA assay was carried out using established protocols as described by Frigerio et al. [26]. In brief, Quanterix Homebrew kit instructions were followed to conjugate beads using recommended buffers and pan-tetraspanin antibodies (anti-CD9, Ancell, clone SN4/C3-3A2, anti-CD63 antibody, Ancell, clone AHN16.1/46–4-5 and anti-CD81 antibody Ancell, clone 1.3.3.22). The three-step assay was performed on 0.1 mL samples that were diluted 1:4 in a diluent and added to a well for capture using conjugated paramagnetic beads. A mixture of biotinylated anti-tetraspanin antibodies (anti-CD9, Ancell, clone SN4/C3-3A2, anti-CD63 antibody, Ancell, clone AHN16.1/46–4-5 and anti-CD81 antibody Ancell, clone 1.3.3.22) was then used to detect the captured EVs. Detection was facilitated by streptavidin-β-galactosidase (SBG), which acted on the fluorogenic substrate resorufin β-D-galactopyranoside (RGP). To establish a calibration curve, serial dilutions of the CPC EV sample, quantified for particle concentration by NTA analysis, were analyzed. For recovery yield calculation, the AEB (Average Enzyme per Bead) raw data for each sample provided by the instrument were first interpolated in the calibration curve to provide a particle concentration, which was then normalized by the volume of the starting material.

2.9. NTA

The NanoSight NS300 system (Malvern Technologies, Malvern, UK) configured with a 532 nm laser was used to perform nanoparticle tracking analysis (NTA) according to the manufacturer's instructions. CPC-EVs were diluted in filtered PBS to a final volume of 1 mL, and ideal measurement concentrations were determined by pre-testing the ideal particle per frame value, ranging from 20 to 100 particles/frame. The manufacturer's software manual was used to adjust the following settings: a syringe pump with constant flow injection was used, and three videos of 60 s were captured and analyzed with NTA software version 3.2. From each video, the mean, mode, and median size of EVs were used to calculate the sample concentration, expressed as nanoparticles/mL.

2.10. Flow cytometry analysis of exosome surface markers

To characterize EVs surface markers, the MACSPlex Exosome Kit (Miltenyi Biotec GmbH) was used following manufacturer's instructions. Briefly, EVs were stained with the capture beads (composed of 39 different bead populations differentially labelled with Fluorescein isothiocyanate − FITC, and Phycoerythrin − PE, and single coated with antibodies specific for 37 different antigens or with 2 isotype control) and the CD9/CD63/CD81 detection antibodies for 1 h on an orbital shaker (450 rpm). For flow cytometry analysis, the MACSQuant Analyzer was used. Triggers for the side scatter and the forward scatter were selected to confine the measurement on the multiplex beads. Voltages for the FITC and PE channels were adapted to ensure that each

of the differentially labelled bead populations were detectable. The 39 single bead populations were gated to allow the determination of the Allophycocyanin (APC) signal intensity (Mean Fluorescence Intensity – MFI) on the respective bead population. Background signals were determined by analysing beads incubated only with detection antibodies and subtracted from the signals obtained for beads incubated with EVs and detection antibodies. A selection of markers with a higher APC fluorescence than isotype controls is shown.

2.11. Electron Microscopy

For Scanning Electron Microscopy (SEM), EVs were fixed with 2.5% glutaraldehyde for 30 min, followed by post- fixation in 1% osmium tetroxide and then dehydrated using a growing series of ethanol dilutions (10% – 100%) and finally air-dried. Samples were mounted with double-faced conductive adhesive tape on metal stub and coated with graphite, and then observed at the SEM (ESEM FEG QUANTA 200, FEI Company, USA).

For Transmission Electron Microscopy (TEM) measurements isolated EVs were adhered on Athene Old 300 mesh copper grids (Agar Scientific, Stansted, Essex, United Kingdom). The sample was fixed with 1% glutaraldehyde, washed 3 times with nuclease free water, and EVs were stained for 5 min with 2% phosphotungstic acid hydrate (Carl Roth, Karlsruhe, Germany). The grids were left to dry and the specimens were visualized using TEM (FEI Tecnai T20, FEI Eindhoven, Netherlands) operated at 160 kV.

3. Results and discussion

3.1. BPt-functionalized HF membrane module

The HF membrane module is comprised of parallel assemblies of PSf HF as illustrated in Fig. 1A. These membranes possess an internal diameter measuring 512 ± 47 μm with a wall thickness of 182 ± 5 μm. SEM analysis of the fiber cross section (Fig. 1B) revealed a porous structure in line with the MW cut-off value (500 kDa). The membranes exhibited a hydraulic permeance of 0.388 L/m^2 h mbar as summarized in Table 1.

HF membranes were modified by a nanometric coating of the Copoly (DMA-NAS-N$_3$-MAPS) (Fig. 2A). This coating was achieved through post-polymerization modification of the base copolymer copoly-(DMA-NAS-MAPS), introducing azido functionality. NMR characterization of

Table 1
Structural and permeability properties of HF membrane module.

NMW cut-off (kDa)	**500**
Internal diameter (μm)	**512 ± 47**
Wall tickness (μm)	**182 ± 5**
Fiber lenght (cm)	**30**
Total area (cm^2)	**26**
Hydraulic permeance (L/m^2 h mbar)	**0.388**

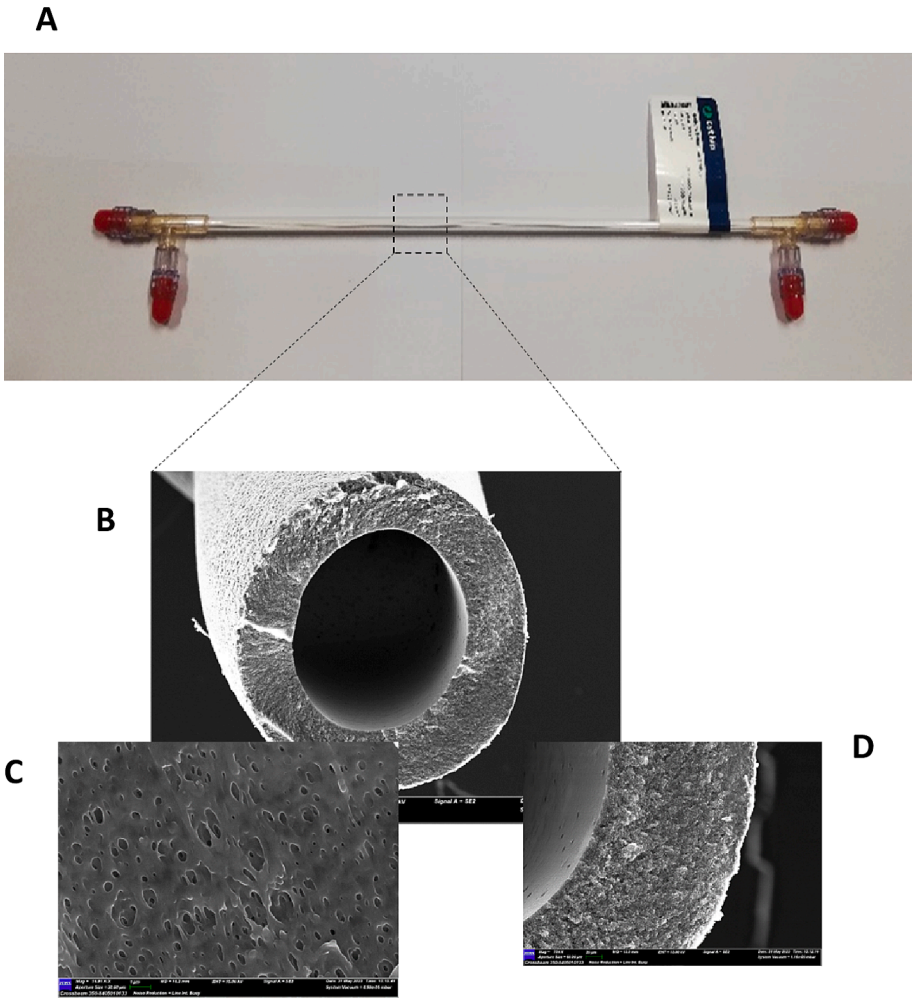

Fig. 1. BPt-functionalized hollow fiber membrane module used in TFF process (A). SEM images of: HF membrane cross section (B), external surface (C) and wall thickness (D).

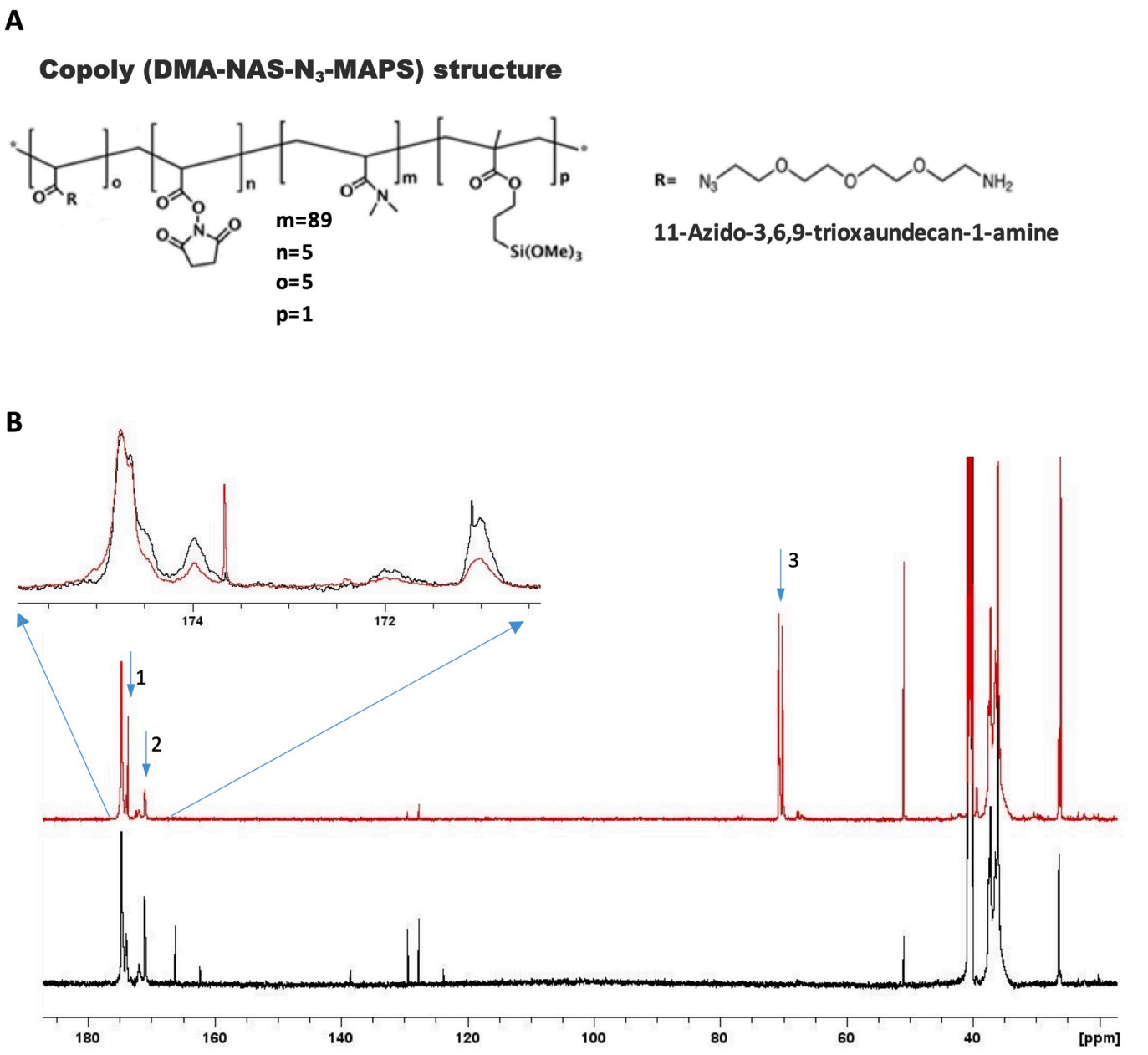

Fig. 2. Composition, monomer fraction and chemical structures of Copoly (DMA-NAS-N_3-MAPS) synthesized for the membrane surface modification (A); ^{13}C NMR spectra of Copoly (DMA-NAS-N_3-MAPS) (red spectra) and Copoly (DMA-NAS-MAPS) (black spectra) (B). In both spectra the presence of two peaks at 174 and 171 ppm (1–2) is related with the carbonyl groups of NAS, instead in the Copoly (DMA-NAS-N_3-MAPS) spectrum the peak at 72 ppm (3) is related to the aliphatic carbons of the PEG linker. (For interpretation of the references to colour in this figure legend, the reader is referred to the web version of this article.)

the synthesised copoly azide polymer revealed distinct features in both spectra. Notably, two peaks at 174 and 171 ppm (1–2) were identified, corresponding to the carbonyl groups of NAS. These signals exhibited a reduction in intensity in the azido modified polymer, suggesting the partial substitution of succinimide groups. Concurrently, the peak at 72 ppm was associated with the aliphatic carbons of the PEG linker, providing evidence for the successful incorporation of the azido linker in the polymeric chain (Fig. 2B). Furthermore, the application of the copolyazide polymer effectively mitigated non-specific interactions, while introducing functional groups for the subsequent conjugation with the peptide BPt (RPPGFSPFR-$(O_2Oc)_2$ −RPPGFSPFR-KG $(O_2Oc)_2$-Prg. The copoly azide polymer coating facilitates the subsequent conjugation of the azide moiety with peptide BPt, resulting in membrane with distinct wettability features and surface free energy parameters. The BPt-functionalized membranes exhibit different polar and apolar characteristics, as reported in Table 2. The Lifshitz–Van Der Waals (γ^{LW}), acid (γ^{+}), base (γ^{-}) and acid–base (γ^{AB}) components of surface tension for both native and functionalized HF membrane were calculated by contact angle measurements in three different reference liquids, according to Good and van Oss' approach [21]. The contact angle values in water and glycerol of the native membranes (θ_W: 79.6° ± 2.0°; θ_{Gly}: 86.06° ± 1.7°) significantly decreased with the BPt functionalization (θ_W: 54.7° ± 3.7°; θ_{Gly}: 71.9° ± 1.9°), while the values in diiodomethane θ_{DIM} increased from 27.3° ± 2.5° on native HF to 37.8° ± 1.6° values for functionalized HF membrane. The BPt functionalization resulted in a decrease of γ^{LW} value indicating a reduction of the apolar properties. A noticeable increase of the base component γ^{-} (28 mJ/m^2), which is representative of the hydrophilic character of surface, is observed after the functionalization compared to the native membrane.

Table 2
Physico-chemical properties of native and copoly azide polymer coated membranes. Contact angles (θ) in water (W), glycerol (Gly), diiodomethane (DIM); γ^{LW}, Lifshitz–van der Waals component, γ^{+}, acid; γ^{-}, base; γ^{AB}, acid–base components of the surface tension γ of the membranes that were calculated according to Good–van Oss equation by the average values of measured contact angle values.

MEMBRANE	θ_W [°]	θ_{Gly} [°]	θ_{DIM} [°]	γ^{LW} [mJ/m^2]	γ^{+} [mJ/m^2]	γ^{-} [mJ/m^2]	γ^{AB} [mJ/m^2]	γ^{tot} [mJ/m^2]
Native PSf	79.6 ± 0.9	86.1 ± 1.7	27.3 ± 2.5	45.2	2.92	16.0	13.7	59.0
c-(DMA-NAS-N_3-MAPS)-BPt	66.5 ± 1.9	79.7 ± 2.0	37.8 ± 4.6	40.7	1.7	28	13.9	54.6

3.2. EVs isolation from conditioned medium of hCPCs

EVs were isolated from conditioned medium of hCPCs through a well-established sequential filtration as outlined previously [20]. This method involves a clarification step, employing dead-end microfiltration to eliminate cell debris and aggregates. Subsequently, ultrafiltration utilizing size based TFF, is employed to isolate EVs from the cell culture components. Simultaneously, this step concentrates the EVs approximately twentythree-fold and eliminates contaminants smaller than the 300 kDa (Fig. 3).

Characterization of EVs in terms of particle size and concentration was conducted using NTA. To assess purification efficiency, concentrations of EVs (quantified by TSG101 levels) and contaminants (free total protein) were analyzed in both the conditioned medium and final EV formulations. Remarkably, the reduction in free proteins exceeded 90%. Additionally, the enrichment of EVs was verified by evaluating the expression of surface markers using a flow cytometer in both the conditioned medium and final EV formulations (see Fig. 4A).

The NTA results show the total particle concentration and size distribution data based on the characteristic movement of particles according to the Brownian motion. The mean size and size mode (most represented size) of EVs were (Mean: 204.6 ± 6.6 nm, Mode: 172.0 ± 8.2 nm), respectively (Fig. 4B). In evaluating the presence of various contaminants (ApoB, ApoA1, ApoA2, Ago2, Calnexin, GRP94, albumin), most of these proteins were found to be below the limit of detection except for albumin which was detected in the EVs solution (16.5 ± 3.8 μg). Notably, the size-based TFF employed did not effectively remove albumin. Therefore, for downstream applications where the presence of albumin could potentially interfere, an additional purification step is advised.

3.3. Selective capture of EVs by BPt-TFF

To achieve the purification and enrichment of a specific range of EVs from the culture medium, BPt-functionalized HF membrane module was integrated in the TFF process. This integration leveraged the size-based transport of species along with specific membrane-sensing ligands. In this process, the feed solution containing EVs (3.3*10^9 part/mL) was

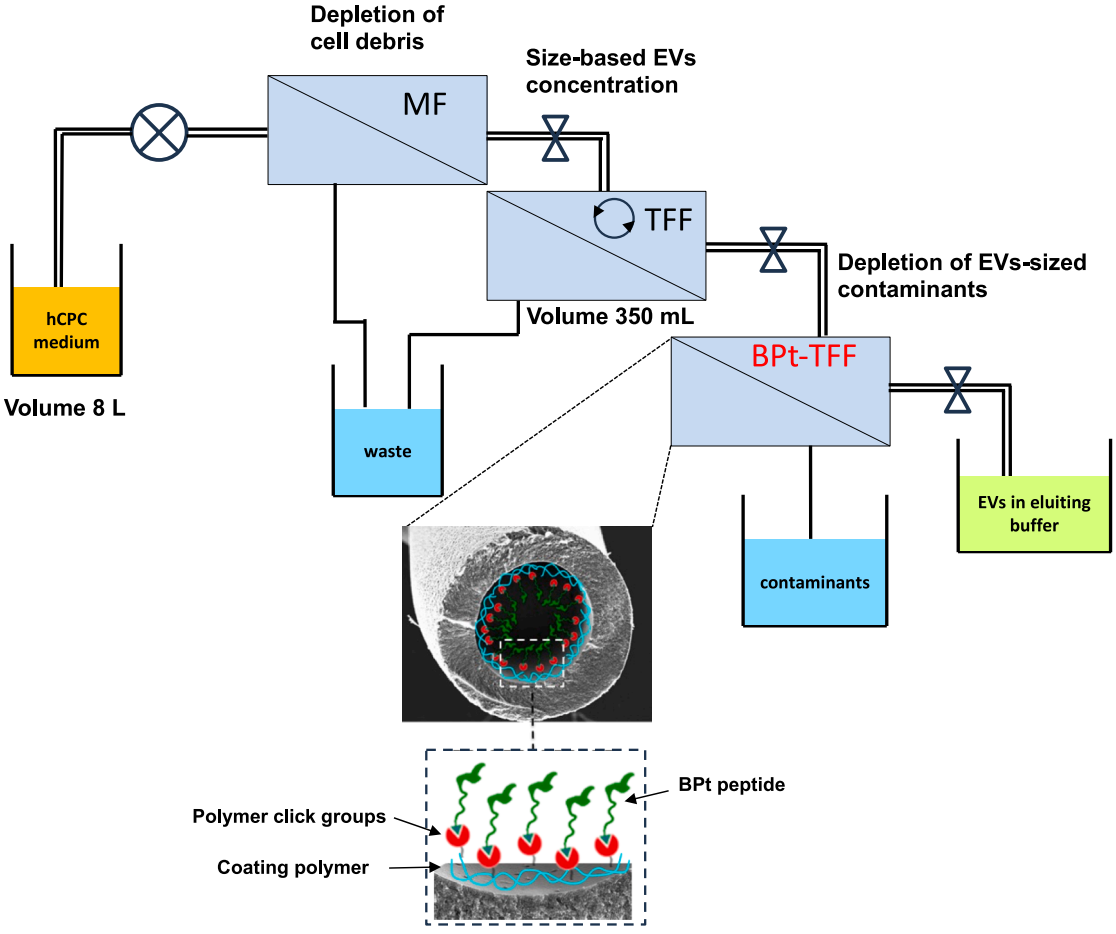

Fig. 3. Schematic of filtration systems for isolation of EVs from hCPC medium. MF: dead-end microfiltration, TFF: tangential flow filtration for size-based EVs separation and concentration, BPt-TFF: BPt-functionalized TFF for selective capture of EVs.

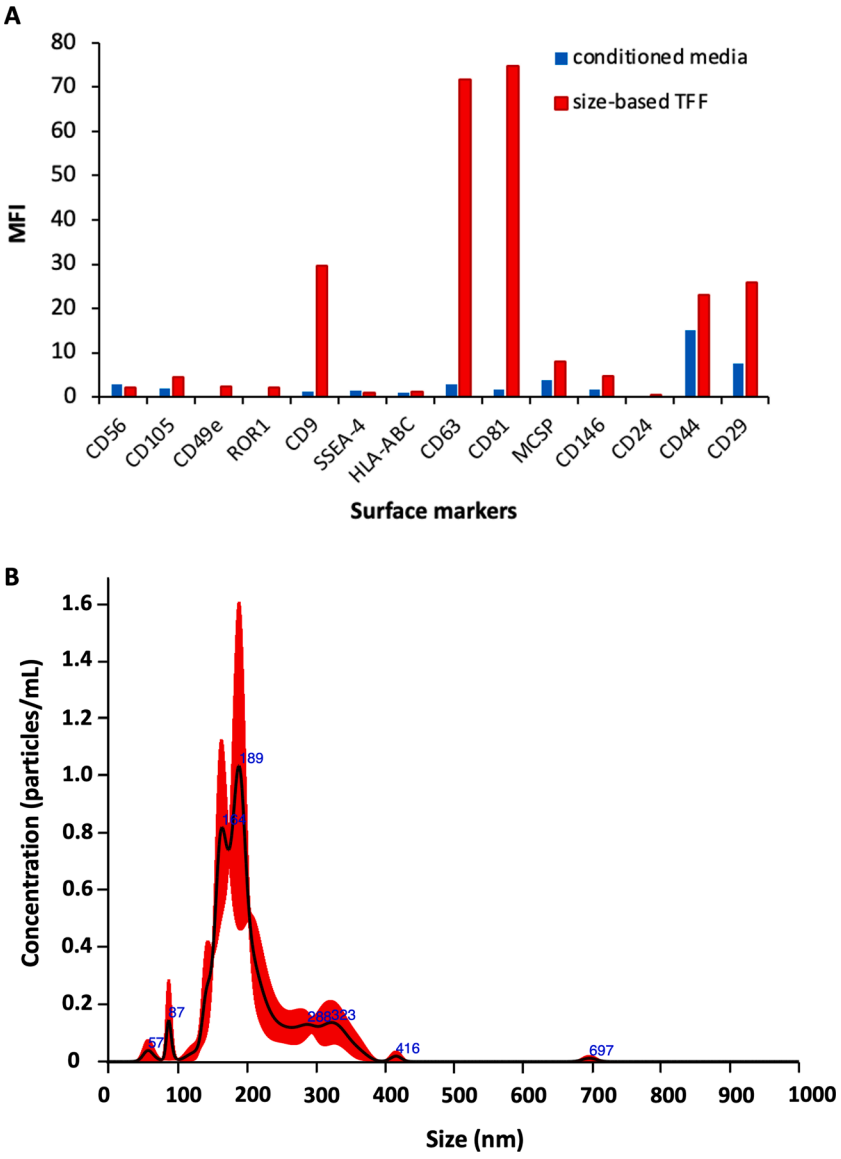

Fig. 4. Extracellular vesicle (EV) marker profile by flow cytometry and nanoparticle tracking analysis. Mean fluorescence intensity (MFI) of different EVs markers by bead-based flow cytometric analysis performed before (conditioned medium) and after the size based TFF isolation (A). Nanoparticle Tracking Analysis (NTA) to determine concentration and size distribution of particles after size-based TFF isolation (B).

tangentially introduced into the membrane lumen. It circulated with low pressure, facilitated by a peristaltic pump, in a closed loop through the reservoir and the hollow fiber membrane module. A portion of the solution permeates the membrane, carrying contaminants (permeate). Simultaneously, EVs were selectively captured into the lumen of membranes, thanks to the specific binding to the BPt peptide immobilized in the lumen. At the same time, the feed volume is reduced and depleted of small EVs (retentate). Operational parameters (e.g., feed, outlet and permeate flow rates) were optimized to ensure a more gentle processing and ultimately, yielding a high output. The feed flow rate of 2 mL/min was set in order to keep low the shear rate (320 s^{-1}) minimizing shear stress. Since it is important to use flow conditions based on relevant physiological reference ranges to preserve EVs integrity, we set-up operating parameters to generate a shear rate value which falls in the human arteries ranges (100–500 s^{-1}) [27]. Thus, the shear rate value in our system is below to those reported in other studies focused on EVs separation and concentration from large volumes of biological fluids [28,29].

The membrane functionalization was designed with the specific goal of eliminating contaminants such as proteins, nucleic acids etc. These contaminants can otherwise interfere with the separation process and purity of the final product. The significance of working with highly purified EV populations is underscored by their potential as precise pharmaceutical targeting vehicles and as sources of diagnostic and prognostic markers. Highly purified vesicle populations are required to define their functionality and diagnostic/therapeutic uses as well as to study the biodistribution and biokinetics [30].

EVs captured into the lumen of membranes were released by treatment with $MgCl_2$ (500 mM). In such condition the metal divalent cation solution was recirculated in the cartridge without permeation for 60 min. Metal cations thanks to their strong coordination ability can interfere with the established interactions between peptide and EVs, allowing their release in the eluting solution [31].

The TFF process with BPt functionalized membrane module led to an enrichment and purification of EVs as shown by Fig. 5. To quantify the EVs bound to the membranes we evaluated the tetraspanins, which are present on EVs but not in lipoproteins or free protein aggregates, and the syntenin that is the most abundant ubiquitous protein associated with exosomes. The transmembrane proteins CD9, CD63, and CD81, and syntenin-1 were detected in the feed, retentate, permeate and $MgCl_2$

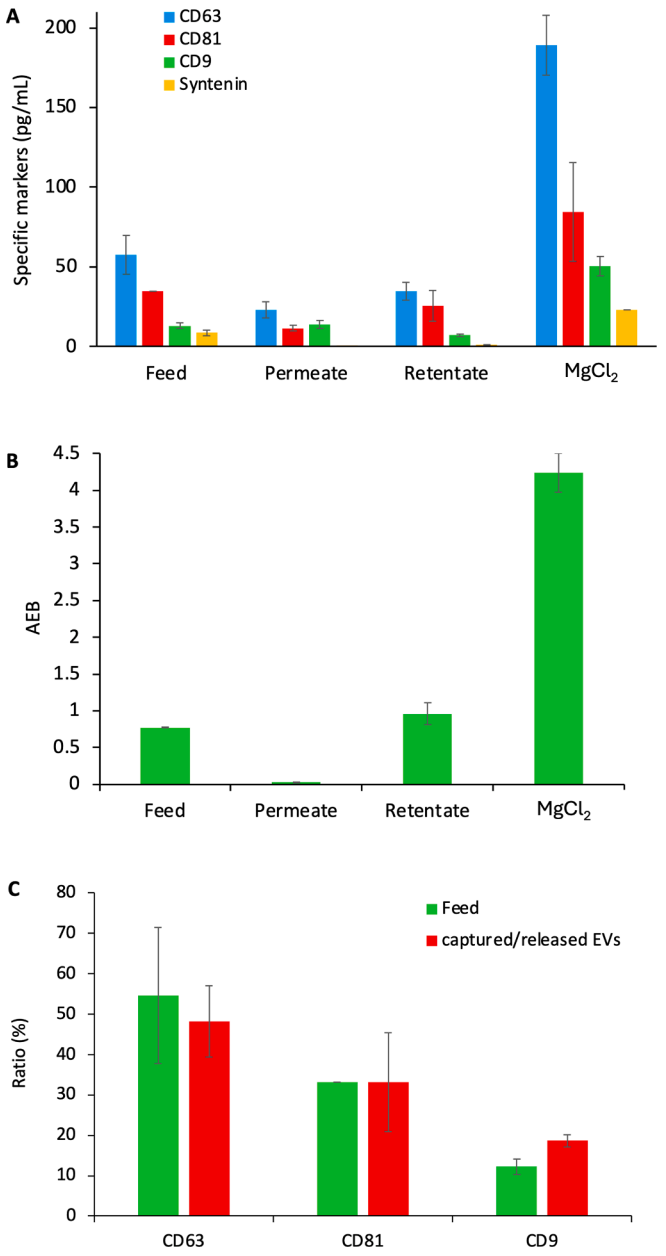

Fig. 5. Characterization of captured and released EVs. (A) ELISA quantitative analysis of tetraspanin CD63, CD81 and CD9, and of syntenin in the feed, permeate, retentate and in the releasing $MgCl_2$ solution. (B) SiMoA data: AEB, average enzyme per bead detected in the feed, retentate, permeate and in the releasing $MgCl_2$ solution. (C) Tetraspanin ratio CD63, CD81 and CD9 in the feed and in the release solution of $MgCl_2$. Values are presented as mean ± SD (n = 3).

eluting solutions. Fig. 5A demonstrated that EVs captured by BPt-functionalized module and released by $MgCl_2$ contain the common EV markers CD63, CD81, CD9 and syntenin-1. Higher amount of the specific markers is detected in the $MgCl_2$ release solution confirming that the concentration process occurred during the TFF, and specific vesicle populations bound by the peptide. SiMoA data (Fig. 5B) corroborated these results demonstrating high selective capturing and release of EVs through BPt-functionalized membrane module.

A similar ratio of the representative EVs surface markers, CD9, CD63, and CD81, was found in the feed and eluting solution highlighting an analogous tetraspanin distribution. CD63 and CD81 were higher expressed than CD9 within the feed and the release solutions (Fig. 5C). This expression pattern is consistent with the quality control check performed on starting material after initial size-exclusion TFF. This finding suggests that the relative EV subfractions composition of the initial preparation is retained during the process. Tetraspanin expression helps to discriminate different subpopulations of EVs, which is important for evaluation of their heterogeneity and specific functional properties [32].

To investigate whether the TFF integrated BPt-functionalized membrane module was able to remove contaminating proteins, experiments were performed to evaluate the content of albumin, which is clearly detected after size-exclusion TFF. Fig. 6 shows the protein contamination of feed solution and the strong decrease of albumin content in the $MgCl_2$ eluting solution suggesting the successful depletion of protein from the released EVs solution. A significant improvement of the EVs purity (93%) was achieved at the end of process. Beside EVs concentration, the TFF membrane process led a significant increase of EVs purity. This represents a breakthrough achievement since the optimization of isolation process in terms of yield and purity became one of the main challenges considering the increasing potential for EVs clinical use. Small sized protein impurities are removed, and EVs can be efficiently isolated and concentrated by using BPt-functionalized membranes integrated in a TFF process overcoming the limitation present in the current isolation methods. Although ultracentrifugation method is considered the “gold standard” for EVs isolation, it is limited by low isolation yield and a high degree of contamination due to the presence of protein aggregates and lipoproteins [33]. Other methods including *SEC* alone has been shown to remove far less efficiently non EVs components such as lipoproteins, thus resulting in preparations of lower purity. Therefore, further purification methods would need to be used to remove contaminants [34]. The size-based TFF process has been introduced to overcome the shortcoming of EVs isolation increasing the separation efficiency according to the cut-off size of membrane. It has been demonstrated that the use of 300 and 500 kDa membranes improved the EVs isolation and the removal of impurities smaller than 40 nm [35]. A cyclic TFF system that includes two membranes with pore sizes of 200 and 30 nm has been proposed to isolate EVs with a specific 30–200 nm size range. However, a purification step after filtration was introduced to remove contaminants for more efficient purification [29].

Moreover, the removal of contaminants may avoid EV aggregation with other complexes increasing their concentration.

The integration of BPt functionalized membrane within the TFF system allows to overcome one of the drawbacks of the current size-based isolation which is the presence of a large number of particles and/or aggregates with the same size of EVs and of other contaminants.

Additionally, this strategy allows the release and delivery of the EVs reverting the peptide-EVs interaction by treatment with divalent metal cations. The released EVs retained round shape morphology and structural integrity as visualized by TEM images (Fig. 7A-B). It is interesting to acknowledge the impact of filtration process has upon EVs, and

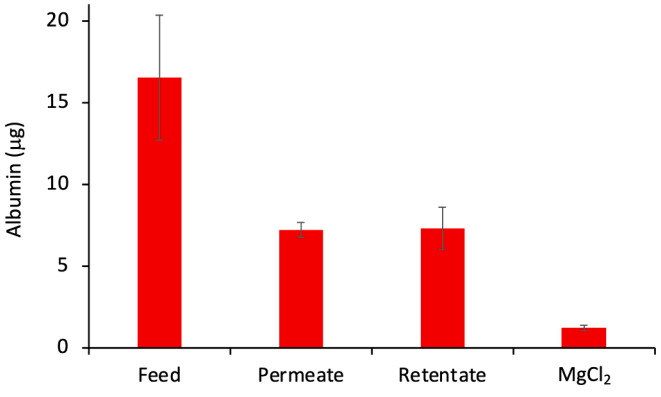

Fig. 6. Amount of albumin detected in the feed, permeate, retentate and in the releasing $MgCl_2$ solution. Values are presented as mean ± SD (n = 3).

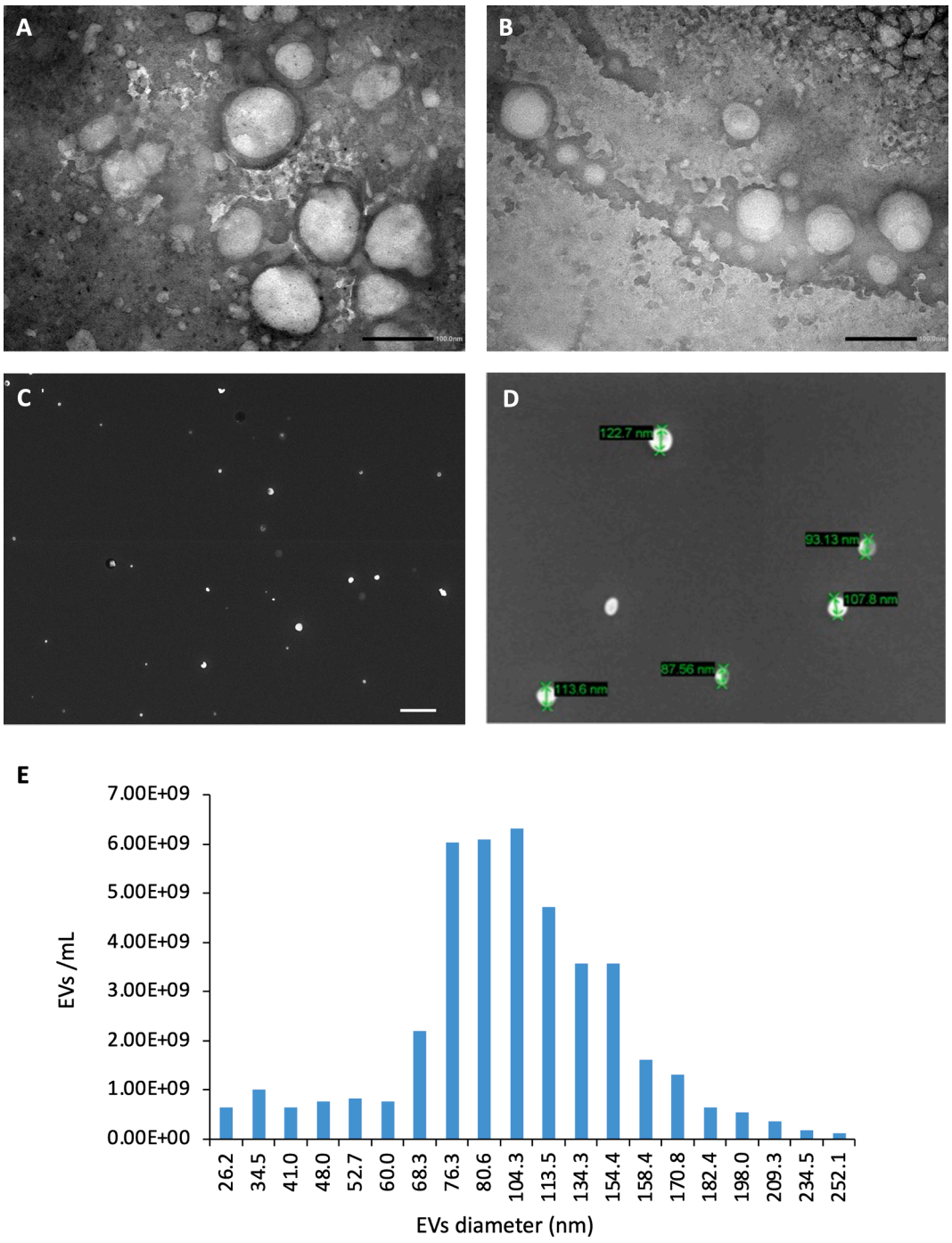

Fig. 7. Images of EVs captured by BPt-functionalized HF membrane during TFF process and released in the $MgCl_2$ solution: (A-B) TEM, scale bar: 100 nm; (C-D) SEM, (C) scale bar: 1 μm, (D) size of the vesicles; (E) size distribution of captured and released EVs under by BPt-TFF conditions. The size distribution was evaluated by Scion Image software analyzing SEM and TEM images of the released EVs.

whether the capture and release process impaired EVs integrity. TEM images showed that EVs isolated were intact and of the expected morphology.

We then measured the size of isolated EVs and as shown in Fig. 7D-E after the first filtration step that involved a size-exclusion TFF, EV sizes were spread over a wide range, from 1 nm to 1000 nm, whereas the size distribution of vesicles after the TFF BPt-functionalized membrane module is more narrow (Fig. 7E). The EVs diameters measured by SEM were ranged from 25 to 250 nm: 98.4% of the captured EVs have a diameter < 200 nm and specifically about 90% display a diameter below 150 nm, only 1.6% of the EVs exhibit a diameter ranged from 200 to 250 nm. Notably, there was an impact on the enrichment of EVs between 60 and 170 nm in diameter without significant losses of EVs.

The use of TFF BPt-functionalized membrane module reduces membrane fouling and the formation of the undesirable adsorption phenomena of non EVs components responsible of the filtration impairment. Furthermore, EVs can be enriched by a process that involves low shear stress, the processing of large volumes with high reliability and reproducibility [29,36]. The process is easily scalable and suitable for the production of GMP-compliant products since it can process volumes from a few mL to a few thousand liters, decreasing non-EV protein and concentrating EVs [37]. Furthermore, the BPt-

functionalized membrane module is selective to specific subpopulations of EVs, and able to handle complex biological fluids.

4. Conclusions

Overall, we proposed a scalable strategy to achieve the separation and enrichment of highly pure EVs combining size-based separation with affinity capture using membrane sensing peptides in a BPt-functionalized HF membrane module, which binds efficiently vesicles characterized by highly curved membranes. This module integrated in a TFF process allowed to capture and to concentrate EVs derived from the conditioned medium of hCPCs efficiently removing contaminants molecules such as albumin. EVs were successfully captured within the lumen of BPt-functionalized HFs and gently released by $MgCl_2$ eluting solution. The BPt-functionalized HF membrane module led to enrichment of EVs with diameter < 200 nm. The captured and released EVs contain the common markers CD63, CD81, CD9 and syntenin-1, and display structural integrity demonstrating the suitability of the system for the selective capture of pure EVs.

CRediT authorship contribution statement

Simona Salerno: Writing – original draft, Methodology, Investigation. **Antonella Piscioneri:** Writing – original draft, Methodology, Investigation. **Sabrina Morelli:** Methodology, Investigation. **Alessandro Gori:** Methodology, Investigation, Conceptualization. **Elena Provasi:** Methodology, Investigation. **Paola Gagni:** Methodology, Investigation. **Lucio Barile:** Writing – review & editing, Validation, Conceptualization. **Marina Cretich:** Writing – review & editing, Conceptualization. **Marcella Chiari:** Writing – review & editing, Conceptualization. **Loredana De Bartolo:** Writing – review & editing, Supervision, Conceptualization.

Declaration of competing interest

The authors declare that they have no known competing financial interests or personal relationships that could have appeared to influence the work reported in this paper.

Data availability

Data will be made available on request.

Acknowledgements

This work was partially funded from the European Union's Horizon 2020 research and innovation program under grant agreements No. 951768 (project MARVEL).

References

[1] S. Morelli, A. Piscioneri, E. Curcio, S. Salerno, C.-C. Chen, L. De Bartolo, Membrane bioreactor for investigation of neurodegeneration, Mater. Sci. Eng. C 103 (2019) 109793, https://doi.org/10.1016/j.msec.2019.109793.

[2] S. Salerno, E. Curcio, A. Bader, L. Giorno, E. Drioli, L. De Bartolo, Gas permeable membrane bioreactor for the co-culture of human skin derived mesenchymal stem cells with hepatocytes and endothelial cells, J. Mem. Sci. 563 (2018) 694–707, https://doi.org/10.1016/j.memsci.2018.06.029.

[3] A. Piscioneri, H.M.M. Ahmed, S. Morelli, S. Khakpour, L. Giorno, E. Drioli, L. De Bartolo, Membrane bioreactor to guide hepatic differentiation of human mesenchymal stem cells, J. Mem. Sci. 564 (2018) 832–841, https://doi.org/10.1016/j.memsci.2018.07.083.

[4] J. Aragón, S. Salerno, L. De Bartolo, S. Irusta, G. Mendoza, Polymeric electrospun scaffolds for bone morphogenetic protein 2 delivery in bone tissue engineering, J. Colloid Interface Sci. 531 (2018) 126–137, https://doi.org/10.1016/j.jcis.2018.07.029.

[5] S. Salerno, A. Messina, F. Giordano, A. Bader, E. Drioli, L. De Bartolo, Dermal-epidermal membrane systems by using human keratinocytes and mesenchymal stem cells isolated from dermis, Mater. Sci. Eng. C Mater. Biol. Appl. 71 (2017) 943–953, https://doi.org/10.1016/j.msec.2016.11.008.

[6] M. Colombo, G. Raposo, C. Thery, Biogenesis, secretion, and intercellular interactions of exosomes and other extracellular vesicles, Annu. Rev. Cell Dev. Biol. 30 (2014) 255–289, https://doi.org/10.1146/annurev-cellbio-101512-122326.

[7] K.M. Candelario, D.A. Steindler, The role of extracellular vesicles in the progression of neurodegenerative disease and cancer, Trends Mol. Med. 20 (2014) 368–374, https://doi.org/10.1016/j.molmed.2014.04.003.

[8] P. Vader, X.O. Breakefield, M.J. Wood, Extracellular vesicles: Emerging targets for cancer therapy, Trends Mol. Med. 20 (2014) 385–393, https://doi.org/10.1016/j.molmed.2014.03.002.

[9] D.A. Borrelli, K. Yankson, N. Shukla, G. Vilanilam, T. Ticer, J. Wolfram, Extracellular vesicle therapeutics for liver disease, J. Control. Release 273 (2018) 86–98, https://doi.org/10.1016/j.jconrel.2018.01.022.

[10] A.J. O'Loughlin, C.A. Woffindale, M.J.A. Wood, Exosomes and the emerging field of exosome-based gene therapy, Curr. Gene Ther. 12 (2012) 262–274, https://doi.org/10.2174/156652312802083594.

[11] S. Gandham, X. Su, J. Wood, A.L. Nocera, S.C. Alli, L. Milane, A. Zimmerman, M. Amiji, A.R. Ivanov, Technologies and standardization in research on extracellular vesicles, Trends Biotechnol. 38 (2020) 1066–1098, https://doi.org/10.1016/j.tibtech.2020.05.012.

[12] D.C. Watson, B.C. Yung, C. Bergamaschi, B. Chowdhury, J. Bear, D. Stellas, A. Morales-Kastresana, J.C. Jones, B.K. Felber, X. Chen, G.N. Pavlakis, Scalable, cGMP-compatible purification of extracellular vesicles carrying bioactive human heterodimeric IL-15/lactadherin complexes, J. Extracell. Vesicles 7 (2018) 1442088, https://doi.org/10.1080/20013078.2018.1442088.

[13] S. Salerno, S. Morelli, A. Piscioneri, M. Frangipane, A. Mussida, L. Sola, R. Frigerio, A. Strada, G. Bergamaschi, A. Gori, M. Cretich, M. Chiari, L. De Bartolo, Multifunctional membranes for lipidic nanovesicle capture, Sep. Purif. Technol. 298 (2022) 121561, https://doi.org/10.1016/j.seppur.2022.121561.

[14] B. Benayas, J. Morales, A. Gori, A. Strada, P. Gagni, R. Frigerio, C. Egea, P. Armisén, M. Cretich, M. Yáñez-Mó, Proof of concept of using a membrane-sensing peptide for sEVs affinity-based isolation, Front. Bioeng. Biotechnol. 11 (2023) 1238898, https://doi.org/10.3389/fbioe.2023.1238898.

[15] A. Gori, A. Romanato, B. Greta, A. Strada, P. Gagni, R. Frigerio, D. Brambilla, R. Vago, S. Galbiati, S. Picciolini, M. Bedoni, G.G. Daaboul, M. Chiari, M. Cretich, Membrane-binding peptides for extracellular vesicles on-chip analysis, J. Extracell. Vesicles 9 (2020) 1751428, https://doi.org/10.1080/20013078.2020.1751428.

[16] L. Sola, F. Damin, P. Gagni, R. Consonni, M. Chiari, Synthesis of clickable coating polymers by postpolymerization modification: applications in microarray technology, Langmuir 32 (2016) 10284–10295, https://doi.org/10.1021/acs.langmuir.6b02816.

[17] L. Sola, D. Brambilla, A. Mussida, R. Consonni, F. Damin, M. Cretich, A. Gori, M. Chiari, A bi-functional polymeric coating for the co-immobilization of proteins and peptides on microarray substrates, Anal. Chim. Acta 1187 (2021) 339138, https://doi.org/10.1016/j.aca.2021.339138.

[18] B. Antonny, Mechanisms of membrane curvature sensing, Annu. Rev. Biochem. 80 (2011) 101–123, https://doi.org/10.1146/annurev-biochem-052809-155121.

[19] G. Andriolo, E. Provasi, A. Brambilla, V. Lo Cicero, S. Soncin, L. Barile, L. Turchetto, M. Radrizzani, GMP-grade methods for Cardiac progenitor cells: cell Bank production and quality control, Methods Mol. Biol. 2286 (2021) 131–166, https://doi.org/10.1007/7651_2020_286.

[20] G. Andriolo, E. Provasi, A. Brambilla, S. Panella, S. Soncin, V.L. Cicero, M. Radrizzani, L. Turchetto, L. Barile, Methodologies for scalable production of high-quality purified small extracellular vesicles from conditioned medium, Methods Mol. Biol. 2668 (2023) 69–98, https://doi.org/10.1007/978-1-0716-3203-1_7.

[21] L. Sola, F. Damin, M. Cretich, M. Chiari, Novel polymeric coatings with tailored hydrophobicity to control spot size and morphology in DNA microarray, Sens. Actuator B Chem. 231 (2016) 412–422, https://doi.org/10.1016/j.snb.2016.03.049.

[22] R.J. Good, C.J. van Oss, The modern theory of contact angles and the hydrogen bond components of surface energies, In: Modern Approaches to Wettability, Springer (1992) 1–27, https://doi.org/10.1007/978-1-4899-1176-6_1.

[23] L. De Bartolo, S. Morelli, A. Bader, E. Drioli, Evaluation of cell behaviour related to physico-chemical properties of polymeric membranes to be used in bioartificial organs, Biomaterials 23 (2002) 2485–2497, https://doi.org/10.1016/s0142-9612(01)00383-0.

[24] G. Andriolo, E. Provasi, V. Lo Cicero, A. Brambilla, S. Soncin, T. Torre, G. Milano, V. Biemmi, G. Vassalli, L. Turchetto, L. Barile, M. Radrizzani, Exosomes from human cardiac progenitor cells for therapeutic applications: development of a GMP-grade manufacturing, Method. Front Physiol. 9 (2018) 1169, https://doi.org/10.3389/fphys.2018.01169.

[25] S. Salerno, F. Tasselli, E. Drioli, L. De Bartolo, Poly(ε-Caprolactone) hollow fiber membranes for the biofabrication of a vascularized human liver tissue, Membranes 10 (2020) 112, https://doi.org/10.3390/membranes10060112.

[26] R. Frigerio, A. Musicò, A. Strada, G. Bergamaschi, S. Panella, C. Grange, M. Marelli, A.M. Ferretti, G. Andriolo, B. Bussolati, L. Barile, M. Chiari, A. Gori, M. Cretich, Comparing digital detection platforms in high sensitivity immune-phenotyping of extracellular vesicles, J. Extracell. Biol. 1 (2022), https://doi.org/10.1002/jex2.53.

[27] M.A. Panteleev, N. Korin, K.D. Reesink, D.L. Bark, J.M.E.M. Cosemans, E. E. Gardiner, P.H. Mangin, Wall shear rates in human and mouse arteries: Standardization of hemodynamics for in vitro blood flow assays: communication from the ISTH SSC subcommittee on biorheology, J. Thromb. Haemost. 19 (2021) 588–595, https://doi.org/10.1111/jth.15174.

[28] G. Corso, I. Mäger, Y. Lee, A. Görgens, J. Bultema, B. Giebel, M.J.A. Wood, J. Z. Nordin, S.E.L. Andaloussi, Reproducible and scalable purification of extracellular vesicles using combined bind-elute and size exclusion

chromatography, Sci. Rep. 7 (2017) 11561, https://doi.org/10.1038/s41598-017-10646-x.
[29] S. Busatto, G. Vilanilam, T. Ticer, W.L. Lin, D.W. Dickson, S. Shapiro, P. Bergese, J. Wolfram, Tangential flow filtration for highly efficient concentration of extracellular vesicles from large volumes of fluid, Cells 7 (2018) 273, https://doi.org/10.3390/cells7120273.
[30] S.P. Kodam, M. Ullah, Diagnostic and therapeutic potential of extracellular vesicles, Technol. Cancer Res. Treat. 20 (2021), https://doi.org/10.3389/fonc.2020.580874, 15330338211041203.
[31] H. Liu, K. Håkansson, Divalent metal ion-peptide interactions probed by electron capture dissociation of trications, J. Am. Soc. Mass Spectrom. 17 (2006) 1731–1741, https://doi.org/10.1016/j.jasms.2006.07.027.
[32] M. Mathieu, N. Névo, M. Jouve, J.I. Valenzuela, M. Maurin, F.J. Verweij, R. Palmulli, D. Lankar, F. Dingli, D. Loew, E. Rubinstein, G. Boncompain, F. Perez, C. Théry, Specificities of exosome versus small ectosome secretion revealed by live intracellular tracking of CD63 and CD9, Nat. Commun. 12 (2021) 4389, https://doi.org/10.1038/s41467-021-24384-2.
[33] J.Y. Kim, W.K. Rhim, Y.I. Yoo, D.S. Kim, K.W. Ko, Y. Heo, C.G. Park, D.K. Han, Defined MSC exosome with high yield and purity to improve regenerative activity, J. Tissue Eng. 12 (2021), https://doi.org/10.1177/20417314211008626, 20417314211008626.
[34] N. Salmond, K.C. Williams, Isolation and characterization of extracellular vesicles for clinical applications in cancer - time for standardization? Nanoscale Adv. 3 (2021) 1830–1852, https://doi.org/10.1039/d0na00676a.
[35] K. Kim, J. Park, J.-H. Jung, R. Lee, J.-H. Park, J.M. Yuk, H. Hwang, J.H. Yeon, Cyclic tangential flow filtration system for isolation of extracellular vesicles, APL Bioeng. 5 (2021) 016103, https://doi.org/10.1063/5.0037768.
[36] R.A. Haraszti, R. Miller, M. Stoppato, Y.Y. Sere, A. Coles, M.C. Didiot, R. Wollacott, E. Sapp, M.L. Dubuke, X. Li, S.A. Shaffer, M. Di Figlia, Y. Wang, N. Aronin, A. Khvorova, Exosomes produced from 3D cultures of MSCs by tangential flow filtration show higher yield and improved activity, Mol. Ther. 26 (2018) 2838–2847, https://doi.org/10.1016/j.ymthe.2018.09.015.
[37] E. Bari, S. Perteghella, D. Di Silvestre, M. Sorlini, L. Catenacci, M. Sorrenti, G. Marrubini, R. Rossi, G. Tripodo, P. Mauri, M. Marazzi, M.L. Torre, Pilot production of mesenchymal stem/stromal freeze-dried secretome for cell-free regenerative nanomedicine: a validated GMP-compliant process, Cells 7 (2018) 190, https://doi.org/10.3390/cells7110190.